

## A novel non-enzyme sensor based on a PDDA-RGO/Pt NPs nanocomposite for electrochemical detection of ascorbic acid

Guanglei Chu<sup>1,2,3</sup>, Guangxian Wang<sup>1,2,3</sup>, Yao Yao<sup>1,2,3</sup>, Xingshuang An<sup>1,2,3</sup>, Yanyan Zhang<sup>\*1,2,3</sup>

<sup>1</sup> School of Agriculture Engineering and Food Science, Shandong University of Technology, No.12 Zhangzhou Road, Zibo 255049, Shandong Province, P.R. China.

<sup>2</sup> Shandong Provincial Engineering Research Center of Vegetable Safety and Quality Traceability, No.12 Zhangzhou Road, Zibo 255049, Shandong Province, PR China.

<sup>3</sup> Zibo City Key Laboratory of Agricultural Product Safety Traceability

\*E-mail: [zyyan1104@163.com](mailto:zyyan1104@163.com)

Received: 26 July 2019 / Accepted: 24 September 2019 / Published: 29 October 2019

---

Enzyme-based sensors exhibit some inevitable shortcomings based on short storage times, poor stability and high cost. In this paper, we used platinum nanoparticles (Pt NPs) instead of enzymes to catalyze the detection of ascorbic acid; thus, we developed a new non-enzymatic sensor electrocatalyst for ascorbic acid detection. Poly dimethyl diallyl ammonium chloride (PDDA)-modified graphene not only showed excellent conductivity and solubility but also increased the modification ability of the nanomaterials. Platinum nanoparticles show a strong catalytic effect on ascorbic acid. By binding both these materials together and modifying them on glassy carbon electrodes, a non-enzymatic sensor based on a PDDA-functionalized reduced graphene oxide-platinum nanoparticles nanocomposite was built. TEM, EDS and FT-IR were used for characterizing the morphology of the samples. The electrochemical properties of the PDDA-reduced graphene oxide-platinum nanoparticles (PDDA-RGO/Pt NPs) electrodes were studied by cyclic voltammetry. The results showed that the sensor could be used to detect AA with excellent electrocatalytic activity, a wide linear range of 0.001 mM-10 mM at 0 V, and a low detection limit of 0.0005  $\mu$ M (S/N=3). The repeatability and stability of the sensor was also studied, and the sensor was found to exhibit excellent performance. From an interference study, it was found that interfering substances had little effect on the sensor, with a recovery rate between 96% and 104% found in actual sample detection. This method of sensor fabrication provided a potential platform for the detection of other biological substances.

---

**Keywords:** Non-enzymic sensor; Platinum nanoparticles; Ascorbic acid detection; Reduced graphene oxide; Poly dimethyl diallyl ammonium chloride

### 1. INTRODUCTION

Ascorbic acid (AA) is an essential substance for health maintenance, and AA shows anti-cancer potential[1], helps treat leukemia[2], and plays essential antioxidant roles in biological systems[3].

Additionally, AA cannot be produced in the human body but is assimilated from external substances, so the accurate and rapid detection of AA is significant[4]. To date, all kinds of detection techniques, such as mass spectrometry (MS)[5], high-performance capillary electrophoresis (HPCE)[6], gas chromatography (GC), fluorimetry[7], spectrophotometry[8], high-performance liquid chromatography (HPLC)[9] and electrochemical methods have been reported. Among these detection methods, the electrochemical method has attracted much attention in the detection of AA by taking advantage of its low cost, simple operation and high sensitivity. However, due to the drawbacks, such as low sensitivity for the direct oxidation of AA shown by traditional sensors and low anti-interference ability and poor reproducibility demonstrated by enzyme sensors, electrochemical sensors show low sensitivity and poor stability for the determination of AA[10, 11]. Therefore, it is urgent to develop electrode materials with good stability, high sensitivity and good selectivity for the detection of AA.

Up to now, although enzyme sensors have been developed rapidly, the cost of enzyme-based sensors remains high, and the detection effect is not stable, mainly because the catalytic activity of enzyme sensors is strongly affected by temperature and pH. Recently, non-enzyme sensors have attracted much attention because of their low cost and good stability.[12] Unlike the enzyme sensor, the catalytic electrode materials of a non-enzyme sensor are mainly based on metals and metal oxides[13].

Developing electrode materials with high conductivity, high catalytic activity and large specific surface area is an important means to improve the performance of electrochemical sensors[14]. Graphene oxide (GO) is a popular nanomaterial for sensors on account of its large specific surface area and excellent electrical conductivity[14-16]. Reduced graphene oxide (RGO) is produced by the reduction of GO. In recent years, graphene-based metal nanocomposites such as, for instance, gold nanoparticles[17], silver nanoparticles[18], magnetic nanoparticles[19] and CuO nanoparticles[20] have been widely studied for use in electrochemical sensors.

However, RGO is easily aggregated by van der Waals interaction, which has adverse effects on its conductivity and catalysis. Poly dimethyl diallyl ammonium chloride (PDDA) is a hydrophilic cationic polymer that is used to prevent RGO recombination through electrostatic interaction and effectively stabilize graphene in water. Therefore, PDDA was used to functionalize graphene. The combined PDDA-RGO has good conductivity and catalytic properties, and the nanomaterials embedded in PDDA-RGO can be directly coated onto a GC electrode without the use of an adhesive[21]. In recent years, platinum nanoparticles have attracted much attention from researchers on account of its large specific surface area, good electrocatalytic activities and high conductivity[22]. The combination of PDDA-reduced graphene oxide-platinum nanoparticles (PDDA-RGO/Pt NPs) shows better electron transfer kinetics, which is largely due to a high surface area and excellent electrocatalytic activity. Therefore, the aim of this work is to design a novel non-enzyme sensor based on a PDDA-functionalized reduced graphene oxide/ platinum nanoparticle nanocomposite for the detection of ascorbic acid.

## 2. EXPERIMENTAL

### 2.1 Reagents

Potassium chloroplatinate ( $K_2PtCl_6$ ) was obtained from the Tianjin Chemical Reagent Research Institute. Graphene oxide was supplied by Nanjing Xianfeng Nano Material Technology Co., Ltd. Ascorbic acid (AA) was purchased from Tianjin Kemiou Chemical Reagent Co., Ltd. Potassium nitrate, potassium ferricyanide, sodium dihydrogen phosphate and disodium phosphate were purchased from the Tianjin Northern Tianyi Chemical Reagent Factory. Poly dimethyl diallyl ammonium chloride (PDDA) and sodium borohydride were obtained from Shandong West Asia Chemical Industry Co., Ltd. Ethanol; potassium ferricyanide and hydrochloric acid were obtained from the Yantai Economic and Technological Development Zone Fine Chemical Plant. Potassium chloride was purchased from Tianjin Yongsheng Fine Chemical Co., Ltd.

### 2.2 Apparatus

Transmission electron microscopy (TEM) images and EDS data were obtained on a Sirion 200 instrument (FEI Hong Kong Limited). Scanning electronic microscopy (SEM) image analysis was performed on a Tecnai G2 Spirit TWIN. Fourier-transform infrared spectroscopy (FT-IR) was carried out on a Nicolet 5700 (Thermo Nicolet Corporation).

Electrochemical measurements were carried out on an electrochemical workstation (CHI 660D, Shanghai Chenhua Instrument Co., Ltd.) with a conventional three-electrode system: glassy carbon was used as the working electrode, with an inner diameter of 4 mm, Ag/AgCl was used as the reference electrode, and platinum wire was used as the counter electrode.

### 2.3 Preparation of PDDA-RGO/Pt NPs

The nanocomposite based on PDDA-RGO/Pt NPs was synthesized by a one-step wet-chemical synthetic route according to a previously reported method that was slightly modified[23]. First, GO (20 mg) was added to deionized water (20 mL) and dispersed by sonication for 2 hours to form a stable solution. Next, the mixture was added into 250  $\mu$ L of potassium chloroplatinate ( $K_2PtCl_6$ , 56 mM). Subsequently, 1 g of freshly prepared sodium borohydride ( $NaBH_4$ ) was added under stirring to form a black graphene oxide/platinum nanoparticle material (RGO/Pt NPs). Then, the mixed material was centrifuged at 10,000 rpm for 30 minutes, and the precipitate was retained. The precipitate was then dissolved with stirring and ultrasonic treatment in a 1% PDDA solution for 1 hour; finally, the sample was centrifuged at 10,000 rpm for 10 minutes to remove the supernatant to retain the precipitate. After the above steps were completed, ethanol and the double distilled water were successively added to the precipitate to perform centrifugal washing under the same conditions, and each step was repeated three times to obtain the PDDA-RGO/Pt NPs composite nanomaterial. Then, PDDA-RGO was prepared by using a similar method.

### 2.4 Fabrication of PDDA-RGO/Pt NP Nanocomposite-Modified Electrodes

First, the working electrode was polished with  $\alpha$ -alumina oxide powder with a size of 0.3  $\mu\text{m}$  and 0.05  $\mu\text{m}$  and then ultrasonically washed with doubly distilled water and ethanol for one minute. To prepare a 2 mg/mL PDDA-RGO/Pt NPs solution, 10 mL of doubly distilled water was added to the prepared material (20 mg PDDA-RGO/Pt NPs) and then ultrasonically treated for 1 hour to obtain the required material. Then, 5  $\mu\text{L}$  of PDDA-RGO/Pt NPs was added onto the GC electrode. After the modified electrode was dried naturally, it was directly used as an electrochemical sensor for AA detection.

## 3. RESULTS AND DISCUSSION

### 3.1 Characteristic Morphologies of the Nanocomposites

TEM, SEM and FI-IR were used to analyze the morphologies of PDDA-RGO and PDDA-RGO/Pt NPs.

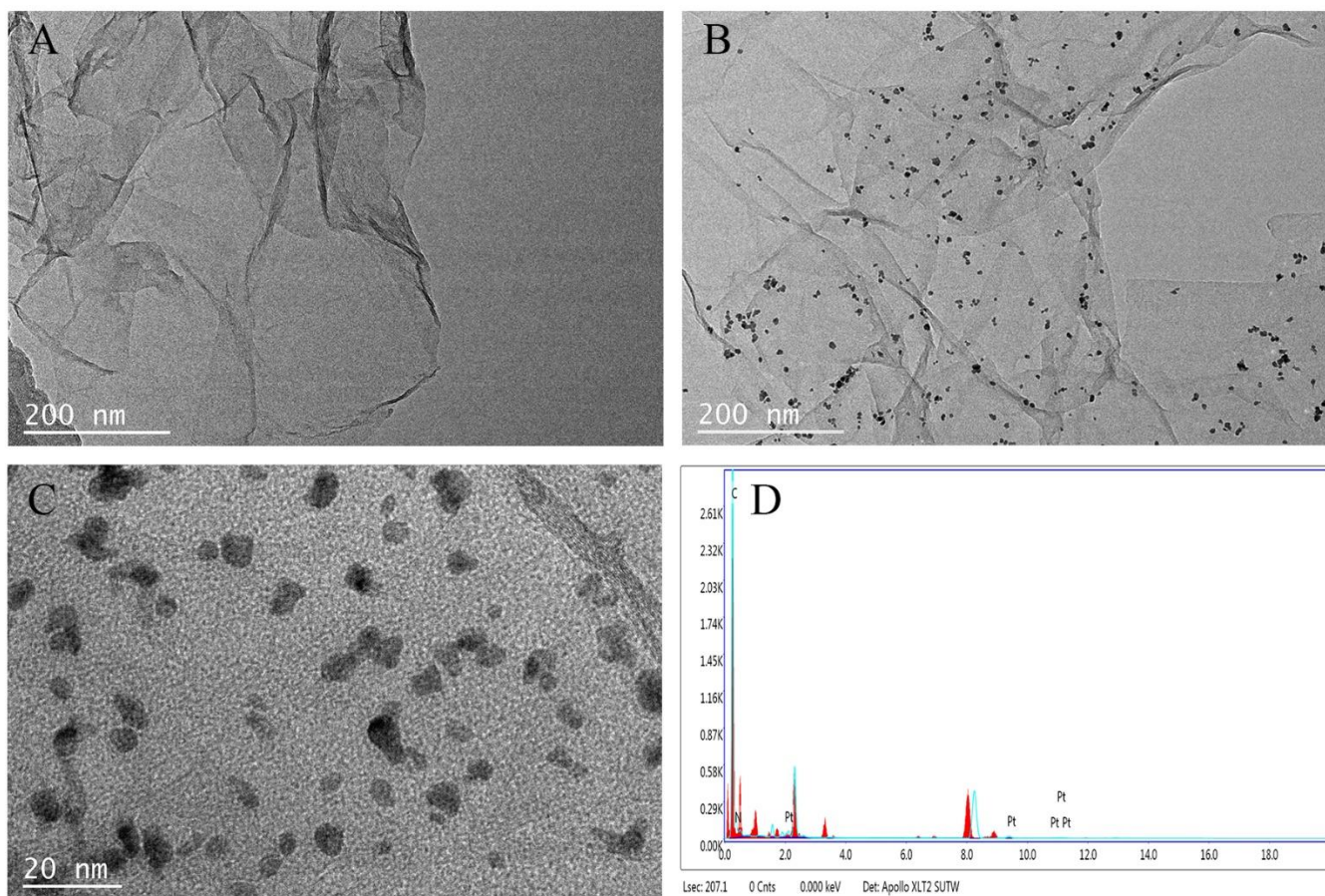


**Figure 1.** (A) TEM images of PDDA-RGO (B, C) and PDDA-RGO/Pt NP nanocomposites under different magnifications, and (D) the EDX spectrum of the PDDA-RGO/Pt NPs

The typical wrinkled form of PDDA-RGO can be seen from Fig. 1A. The graphene oxide showed a color change from brown to black, which also indicated that the reduction of the graphene oxide was successful[21, 24]. In addition, as shown in Fig. 1B, Pt NPs were well-dispersed onto the lamellar surface of RGO, indicating that PDDA-RGO played a crucial role in promoting the uniform dispersion of Pt NPs and avoided the aggregation of Pt NPs. The diameters of the Pt NPs showed good uniformity and were concentrated to a range of 3-5 nm, as shown in Fig. 1C. EDX (Fig. 1D) analysis showed that the PDDA-RGO/Pt NPs were composed of C, N and Pt elements, with N being derived from PDDA. The above characterization images indicated that the PDDA-RGO/Pt NPs nanomaterials were prepared successfully.

Fig. 2A shows the FT-IR spectra for the GO (a) and PDDA-RGO/Pt NPs (b). The GO spectrum illustrates the appearance of a broad O-H peak ( $V_{O-H}$  at  $3414\text{ cm}^{-1}$ ) and peaks for C=O ( $V_{C=O}$  at  $1732\text{ cm}^{-1}$ ), aromatic C=C ( $V_{C=C}$  at  $1627\text{ cm}^{-1}$ ), C-OH ( $V_{C-OH}$  at  $1384\text{ cm}^{-1}$ ), C-O-C ( $V_{C-O-C}$  at  $1127$ ) and alkoxy C-O ( $V_{C-O}$  at  $1053\text{ cm}^{-1}$ )[24, 25]. In contrast to the GO, the typical C=O absorption bands at  $1732\text{ cm}^{-1}$  and the C-OH absorption bands at  $1384\text{ cm}^{-1}$  for GO-Pt almost disappear, indicating that the carbonyl groups on the surface of the GO sheets were modified by Pt NPs. The peak intensities at  $3414\text{ cm}^{-1}$  and  $1053\text{ cm}^{-1}$  were dramatically decreased, which indicated that the O-H and C-O bands for GO disappear after  $\text{NaBH}_4$  reduction. Based on the above results, the successful preparation of nanocomposites was further proven, which was consistent with the results from TEM and EDX.

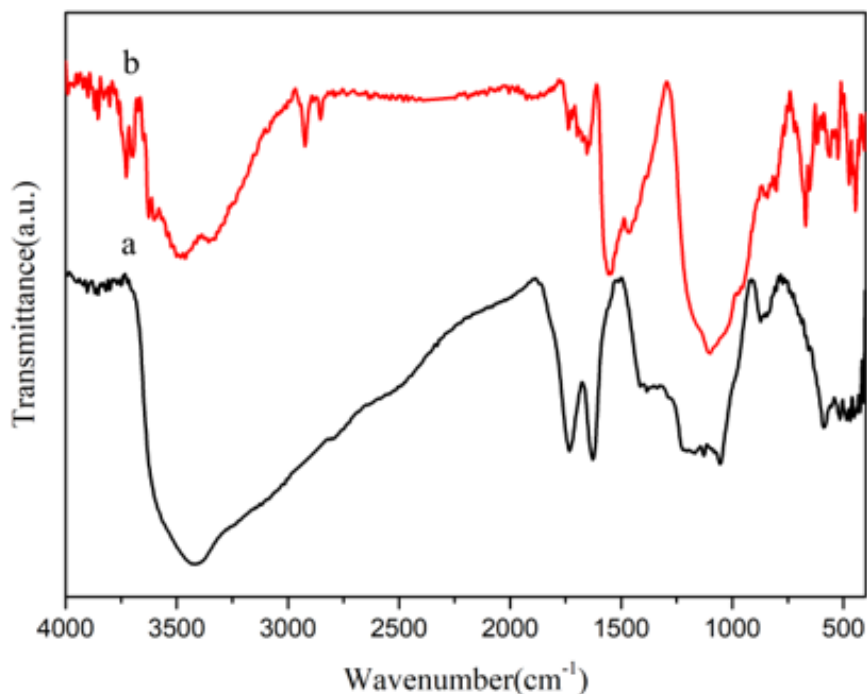


**Figure 2.** FT-IR spectra for GO(a) and PDDA-RGO/Pt NPs

### 3.2. Electrochemical Characterization of the Fabricated sensor

The cyclic voltammetry (CV) images of the PDDA-RGO electrode and PDDA-RGO-Pt NPs electrode were compared with that of a bare GC electrode, which were obtained in 0.1 M KCl with

10 mM  $[\text{Fe}(\text{CN})_6]^{3-}$ . The GC electrode showed a couple of well-defined redox peaks; the modified PDDA-RGO electrode showed a greater current response with a peak current of  $90.2 \mu\text{A}$ , which suggested that PDDA-RGO favored an enhancement of the electrical signals. The PDDA-RGO/Pt NPs nanocomposite showed an obvious increase in the peak current to  $147.4 \mu\text{A}$ , which was ascribed to the synergistic effect of the PDDA-RGO and Pt NPs. This result proved that the PDDA-RGO /Pt NPs modified electrode had good electrochemical characteristics, which laid a solid foundation for the sensitive and rapid detection of AA in the future.

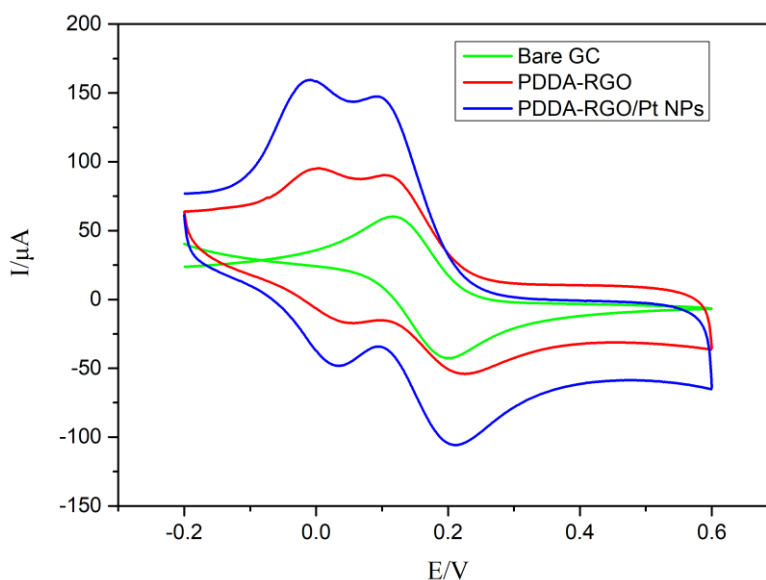


**Figure 3.** CVs for the bare GCE and for the PDDA-RGO and PDDA- PDDA-RGO/Pt NPs electrodes recorded in 0.1 M KCl solution containing 10 mM  $[\text{Fe}(\text{CN})_6]^{3-}$ . Scan rate:  $50 \text{ mVs}^{-1}$

### 3.3. Electrochemical Response of the Fabricated Sensor to AA

To verify the response of the sensor to AA, the fabricated sensor was used to detect AA in 0.1 M PBS (pH=7) by cyclic voltammetry. Fig. 4A shows the electrochemical reaction of the PDDA-RGO /Pt NP/GC electrode in 0.1 M PBS (pH=7) solution with 20 mM AA (a) and no AA (b). There was no obvious anode current peak in the measured curve (b), but there was an obvious anode current peak ( $159 \mu\text{A}$ ) in the curve (a) at 0 mV. This finding indicated that the prepared sensor possessed an excellent catalytic property for AA of approximately 0 mV. The above results are consistent with the previously reported literature[26, 27].

Fig. 4B shows the cyclic voltammetry (CV) for the bare GC electrode (a), PDDA-RGO/GC electrode (b), and PDDA-RGO/Pt NPs/GC electrode (c) in 0.1 M PBS with 10 mM AA measured at a scan rate of  $50 \text{ mVs}^{-1}$ . As seen from the figure, curves (a) and (b) show no redox peak; nevertheless, a significant anode current peak is observed for the PDDA-RGO/Pt NP/GC electrode at 0 mV. As a result, the Pt NPs are a superior material for catalyzing ascorbic acid.

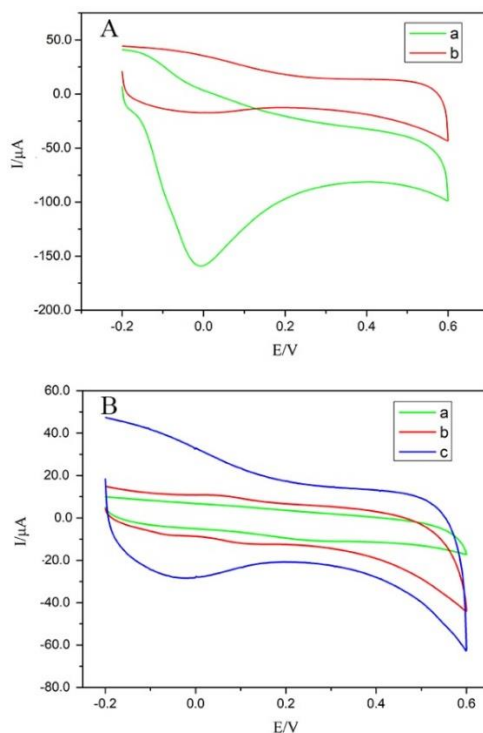


**Figure 4.** (A) The electrochemical reaction of the PDDA-RGO/Pt NP/GC electrode in 0.1 M PBS (pH 7) solution with the absence (a) and presence (b) of 20 mM AA; (B) CVs for the bare GC electrode (a), PDDA-RGO/GC electrode (b), and PDDA-RGO/Pt NP/GC electrode (c) in 0.1 M PBS with 10 mM AA

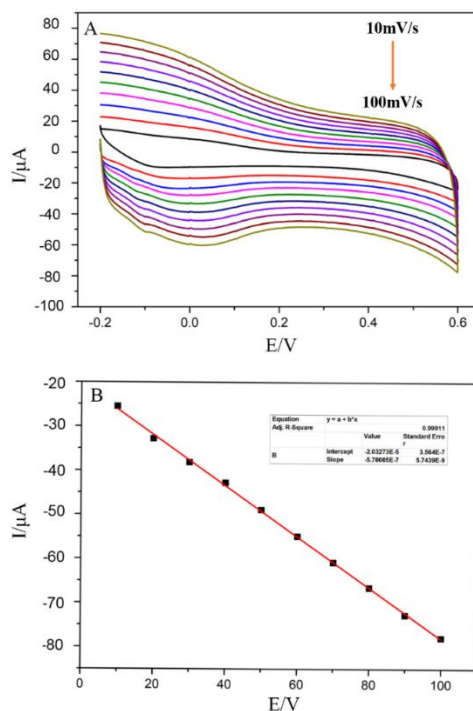


**Figure 5.** (A) CVs for the PDDA-RGO/Pt NPs/GC electrode in 0.1 M PBS (pH 7.0) with 10 mM AA at varying scan rates: 10 mVs<sup>-1</sup>, 20 mVs<sup>-1</sup>, 30 mVs<sup>-1</sup>, 40 mVs<sup>-1</sup>, 50 mVs<sup>-1</sup>, 60 mVs<sup>-1</sup>, 70 mVs<sup>-1</sup>, 80 mVs<sup>-1</sup>, 90 mVs<sup>-1</sup> and 100 mVs<sup>-1</sup>; (B) The plot of the cathodic peak current values against the scan rate.

To elucidate the electrochemical kinetics of the PDDA-RGO/Pt NPs modified sensor toward ascorbic acid, the effect of the scanning rate on electrochemical performance was studied. Fig. 5A shows that the anode current increased with increasing scanning rate from  $10 \text{ mV/s}^{-1}$  to  $100 \text{ mV/s}^{-1}$  in PBS (pH 7.0) containing 10 mM AA. As shown in Fig. 5B, a linear relationship exists between the anode peak current and the scanning rate ( $R^2=0.999$ ). In conclusion, the detection of AA conformed to surface adsorption kinetics.

#### 3.4. The effect of pH

The pH of the buffer has an impact on the current response of the modified electrode. The peak currents for PBS buffers with different pH values were tested with 5 mM AA. Fig. 6 shows that the anode current increases as the pH increases from 4.0 to 7.0 but decreases as the pH increases from 7.0 to 8.0, and this difference may be due to the influence of excessive acid and alkali destroying the structure of AA. Therefore, in the following experiment, we chose a pH 7.0 PBS buffer as the supporting solution.

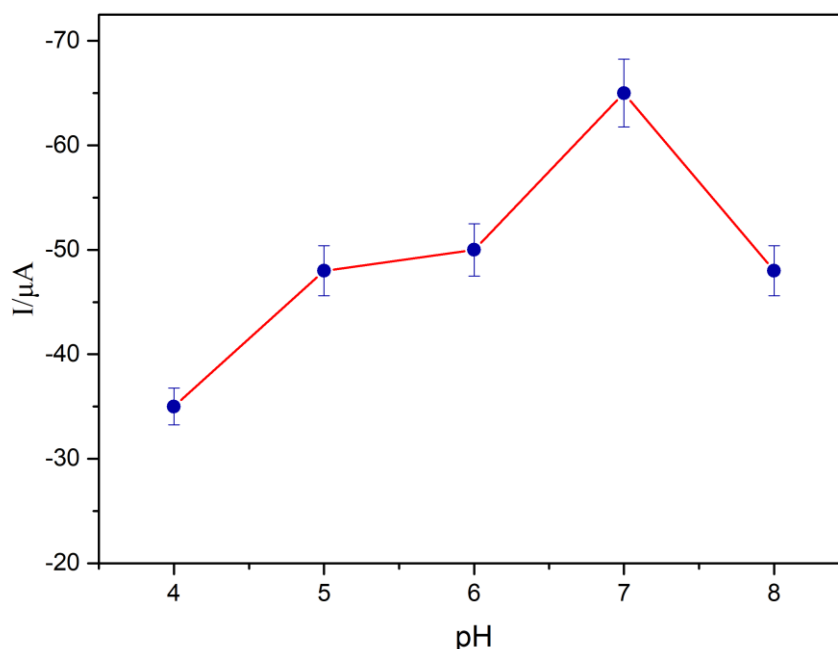


**Figure 6.** The effect of pH on the current response of 5 mM AA in 0.1 M PBS

#### 3.5. Electrochemical Detection of the Prepared Sensor for AA Detection

The current response of the non-enzyme sensor for detecting AA was measured by CV under optimal conditions. The cyclic voltammetry for the PDDA-RGO/Pt NPs/GC modified electrodes for detecting ascorbic acid in the range of 0.001 mM to 10 mM (pH 7.0) at  $50 \text{ mV/s}^{-1}$  is shown in Fig. 7A. As seen from the figure, as the concentration of ascorbic acid is increased, the current signal due to ascorbic acid increased steadily. In addition, as shown in Fig. 7B, the current response in the range of 0.001 mM to 10 mM was proportional to the ascorbic acid concentration. Upon fitting the data, we

found the linear regression equation to be  $E_{pa}(\mu A) = -20.189 - 9.45498C$ , with a correlation coefficient ( $R^2$ ) of 0.995. The detection limit was calculated by using  $3 \times \text{blank variance/slope}$  ( $S/N=3$ ) and was found to be 0.05 nM, which is much lower than many previously reported sensors (Table 1). The sensor exhibits superior performance and provides a promising platform for monitoring living bodies.

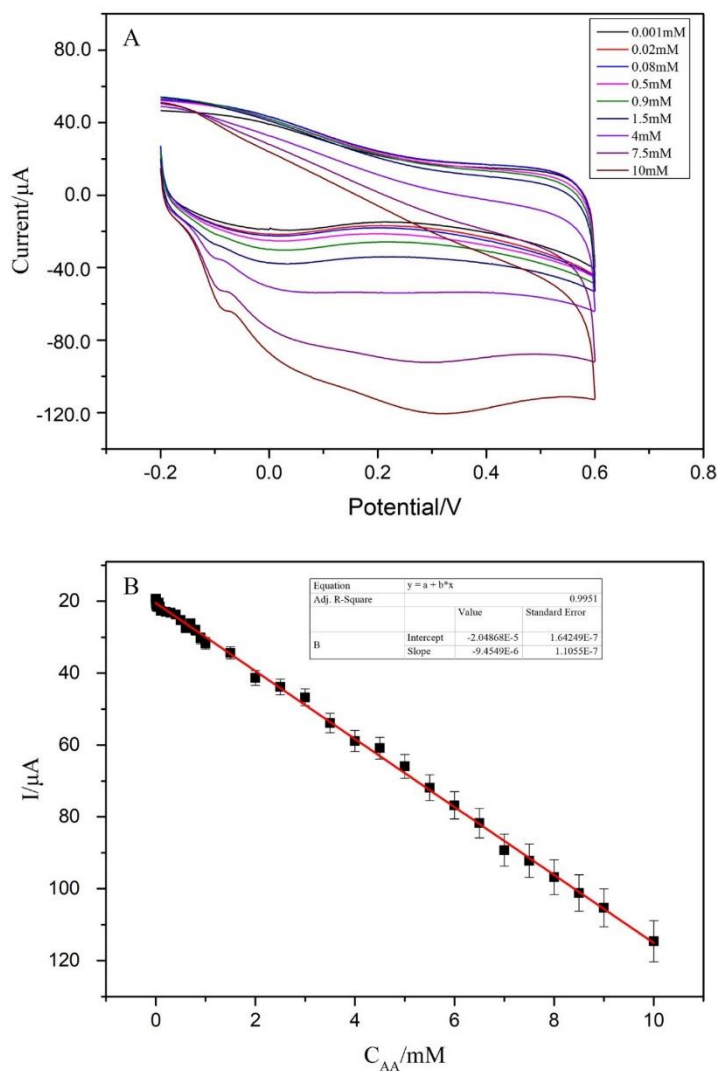


**Figure 7.** CV of the PDDA-RGO /Pt NPs/GC electrodes for detecting ascorbic acid at concentrations ranging from 0.008 mM to 10 mM in 0.1 M PBS (pH 7.0) at 50 mV

For comparison, Table 1 lists the lowest detection limit and linear ranges of recently published methods or electrode materials for the detection of AA. In comparison, the PDDA-RGO/Pt NPs electrodes exhibited superior performance for AA detection. The excellent performance of the sensor may benefit from the synergistic effect of the PDDA-RGO and Pt NPs, which effectively increased the electron transfer on the electrode surface and improved the electrocatalytic activity against ascorbic

acid. Therefore, this new type sensor is expected to be used in the detection of ascorbic acid in living bodies.

**Table 1.** Comparison of different materials or methods used for detecting ascorbic acid

Methods	Electrode material	Linear range ( $\mu\text{M}$ )	Detection limit ( $\mu\text{M}$ )	References
Fluorescence	M-CQDs	10-70 $\mu\text{M}$	3.26 $\mu\text{M}$	[28]
Fluorescence	GSH-AuNCs	350-700 $\mu\text{M}$ .	200 $\mu\text{M}$	[29]
Electrochemistry	ZnNi NPs@f-MWCNT	300-1100 $\mu\text{M}$	0.51 $\mu\text{M}$ .	[30]
Colorimetry	GoldMag	10-1000 $\mu\text{M}$	0.12 $\mu\text{M}$	[31]
Electrochemistry	BN/GCE	30–1000 $\mu\text{M}$	3.77 $\mu\text{M}$	[32]
Electrochemistry	CL-TiN/GCE	50–1500 $\mu\text{M}$	1.52 $\mu\text{M}$	[33]
Electrochemistry	GCE/CNO/Thionine	0-50 $\mu\text{M}$	0.66 $\mu\text{M}$	[34]
Electrochemistry	PDDA-RGO/Pt NPs	1-10000 $\mu\text{M}$	0.0005 $\mu\text{M}$	This work

### 3.5. Reproducibility and Stability of the Sensor

The stability and reproducibility of the sensor was also evaluated. Five electrodes modified with the PDDA-RGO /Pt NPs nanocomposite were tested for reproducibility. By measuring the anode peak current in 1 mM AA, the relative deviation was determined to be 3.7%. In addition, the stability of the sensor was evaluated by measuring the response current for 1 mM AA every five days for one month. After 30 days, the sensor still maintained 91.5% of the initial current response (Fig. 8). Therefore, the above results indicated that the sensor showed good reproducibility and long-term stability.

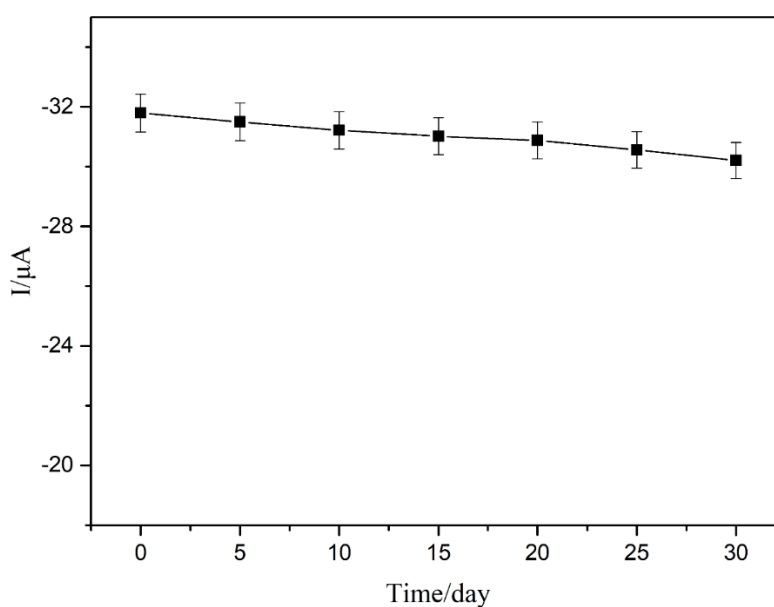


**Figure 8.** The long-term stability of the non-enzymatic AA sensor

### 3.6 Interference Studies and Real Sample analysis

For studying possible interference against ascorbic acid detection, a 0.1 M PBS (pH=7.0) solution with only 1 mM ascorbic acid and 1 mM ascorbic acid solution mixed with 0.1 mM hydrogen peroxide, 0.1 mM dopamine and 0.1 mM glucose was used for cyclic voltammetry. As shown in Fig. 9, the electrochemical response with only 1 mM ascorbic acid (a) was almost unchanged compared with the electrochemical response with three interferences (b). However, a reduction peak was observed with a current of  $-26.97 \mu\text{A}$  near 0.16 V, probably due to the effect of dopamine[35].

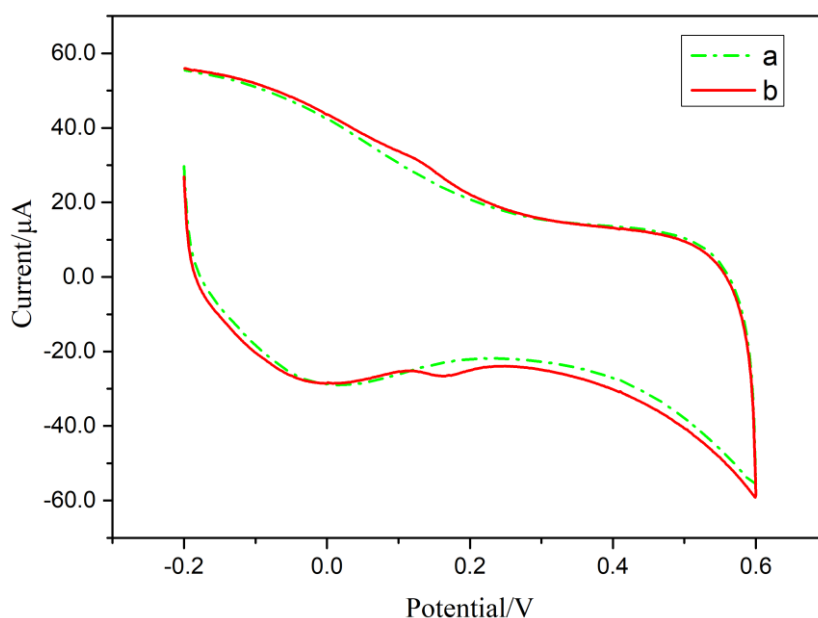


**Figure 9.** CV of 1 mM AA (a) and a solution of 1 mM AA mixed with 0.1 mM glucose, 0.1 mM dopamine and 0.1 mM hydrogen peroxide (b) in 0.1 M PBS (pH 7.0).

To verify the practical application performance of the prepared non-enzyme AA sensor, the sensor was used to detect the amount of AA in tomatoes. As shown in Table 2, for this test, the recovery rate ranged between 96-104%, and the relative standard deviation ranged between 3%-4%. The sensor shows promising performance for the detection of AA in actual samples.

**Table 2.** Determination of the AA concentration in tomato samples (n=6).

Sample	AA added (mM)	AA found (mM)	Recovery (%)	R.S.D. (%)
1	0.050	0.048	96.0	4.15
2	0.120	0.118	98.3	3.96
3	0.850	0.870	102.4	4.03
4	2.500	2.600	104.0	3.66
5	5.000	4.850	97.0	3.78

#### 4. CONCLUSION

In this study, a PDDA-RGO /Pt NP nanocomposite was prepared by a simple and efficient method; by modifying the nanocomposite on a GC electrode, a novel non-enzyme AA sensor with high sensitivity and selectivity was successfully prepared. The sensor was used for the detection of AA and exhibited high electrocatalytic activity, high sensitivity, a wide detection range, and a low detection limit. Compared with other nanomaterials, PDDA-RGO/Pt NPs nanocomposites have obvious advantages. Moreover, the non-enzyme sensor greatly improved the catalytic performance and showed satisfactory performance, which was mainly attributed to the synergistic effect of the PDDA-RGO and Pt NPs. With the excellent performance of the PDDA-RGO /Pt NPs, the nanocomposite can be used to prepare non-enzyme sensors for AA detection, which provides a promising platform for substance detection in a living body.

#### ACKNOWLEDGMENTS

This work was supported by the Foundation of Shandong Provincial (ZR2018BC055)

#### References

1. C.-N. Zhao, Y. Li, X. Meng, S. Li, Q. Liu, G.-Y. Tang, R.-Y. Gan, H.-B. Li, *Cancer Lett.*, 431 (2018) 161-170.
2. L. Cimmino, I. Dolgalev, Y. Wang, A. Yoshimi, G.H. Martin, J. Wang, V. Ng, B. Xia, M.T. Witkowski, M. Mitchell-Flack, I. Grillo, S. Bakogianni, D. Ndiaye-Lobry, M.T. Martin, M. Guillaumot, R.S. Banh, M. Xu, M.E. Figueroa, R.A. Dickins, O. Abdel-Wahab, C.Y. Park, A. Tsirigos, B.G. Neel, I. Aifantis, *Cell*, 170(6) (2017) 1079-1095.
3. B.M.M. May, S. Parani, O.S. Oluwafemi, *Mater. Letter*, 236 (2019) 432-435.
4. P.E. Marik, *Pharmacol. Ther.*, 189 (2018) 63-70.
5. S.M. Wabaidur, Z.A. Alothman, M.R. Khan, *Spectrochim. Acta., Part A*, 108 (2013) 20-5.
6. M.T. Falkova, A.V. Bulatov, M.O. Pushina, A.A. Ekimov, G.M. Alekseeva, L.N. Moskvina, *Talanta*, 133 (2015) 82-7.
7. L. Wang, L. Zhang, S. She, F. Gao, *Spectrochim. Acta., Part A*, 61(11-12) (2005) 2737-40.
8. Y. Bazel, T. Riabukhina, J. Tirpák, *Microchem. J.*, 143 (2018) 160-165.
9. F. Turak, R. Guzel, E. Dinc, *J Food Drug Anal*, 25(2) (2017) 285-292.
10. Y. Zhang, P. Liu, S. Xie, M. Chen, M. Zhang, Z. Cai, R. Liang, Y. Zhang, F. Cheng, *J. Electroanal. Chem.*, 818 (2018) 250-256.
11. D. Huang, X. Li, M. Chen, F. Chen, Z. Wan, R. Rui, R. Wang, S. Fan, H. Wu, *J. Electroanal. Chem.*, 841 (2019) 101-106.
12. W.C. Lee, K.B. Kim, N.G. Gurudatt, K.K. Hussain, C.S. Choi, D.S. Park, Y.B. Shim, *Biosens. Bioelectron.*, 130 (2019) 48-54.
13. D.W. Hwang, S. Lee, M. Seo, T.D. Chung, *Anal. Chim. Acta*, 1033 (2018) 1-34.
14. C. Zhang, Y. Zhang, X. Du, Y. Chen, W. Dong, B. Han, Q. Chen, *Talanta*, 159 (2016) 280-286.
15. N. Mohammadian, F. Faridbod, *Sens. Actuators, B*, 275 (2018) 432-438.
16. Z. Zhou, C. Gu, C. Chen, P. Zhao, Y. Xie, J. Fei, *Sens. Actuators, B*, 288 (2019) 88-95.
17. H.R. Akbari Hasanjani, K. Zarei, *Biosens. Bioelectron.*, 128 (2019) 1-8.
18. L. Kashefi-Kheyraadi, M.A. Mehrgardi, *Biosens. Bioelectron.*, 37(1) (2012) 94-8.
19. N. Ben Messaoud, A. Ait Lahcen, C. Dridi, A. Amine, *Sens. Actuators, B*, 276 (2018) 304-312.
20. D. Xu, C. Zhu, X. Meng, Z. Chen, Y. Li, D. Zhang, S. Zhu, *Sens. Actuators, B*, 265 (2018) 435-442.
21. J. Yang, Q. Lin, W. Yin, T. Jiang, D. Zhao, L. Jiang, *Sens. Actuators, B*, 253 (2017) 1087-1095.

22. E. Teran-Salgado, D. Bahena-Urbe, P.A. Márquez-Aguilar, J.L. Reyes-Rodriguez, R. Cruz-Silva, O. Solorza-Feria, *Electrochim. Acta*, 298 (2019) 172-185.
23. J. Guo, R. Wang, W.W. Tjiu, J. Pan, T. Liu, *J. Hazard. Mater.*, 225-226 (2012) 63-73.
24. Y. Yu, Z. Chen, B. Zhang, X. Li, J. Pan, *Talanta*, 112 (2013) 31-6.
25. C. Zhang, Y. Zhang, Z. Miao, M. Ma, X. Du, J. Lin, B. Han, S. Takahashi, J.-i. Anzai, Q. Chen, *Sens. Actuators, B*, 222 (2016) 663-673.
26. A. Kumar, J.S.G. Selva, J.M. Gonçalves, K. Araki, M. Bertotti, *Electrochim. Acta*, 322 (2019).
27. N.F. Atta, A. Galal, Y.M. Ahmed, E.H. El-Ads, *Sens. Actuators, B*, 297 (2019).
28. S. Chandra, V.K. Singh, P.K. Yadav, D. Bano, V. Kumar, V.K. Pandey, M. Talat, S.H. Hasan, *Anal. Chim. Acta*, 1054 (2019) 145-156.
29. X. Yan, L. He, C. Zhou, Z.-J. Qian, P. Hong, S. Sun, C. Li, *Chem. Phys.*, 522 (2019) 211-213.
30. A. Savk, B. Ozdil, B. Demirkan, M.S. Nas, M.H. Calimli, M.H. Alma, Inamuddin, A.M. Asiri, F. Sen, *Mater. Sci. Eng., C*, 99 (2019) 248-254.
31. H. Guan, B. Han, D. Gong, Y. Song, B. Liu, N. Zhang, *Spectrochim. Acta, Part A*, 222 (2019) 117277.
32. Q. Li, C. Huo, K. Yi, L. Zhou, L. Su, X. Hou, *Sens. Actuators, B*, 260 (2018) 346-356.
33. L. Zhang, J. Feng, K.-C. Chou, L. Su, X. Hou, *J. Electroanal. Chem.*, 803 (2017) 11-18.
34. J.P. Bartolome, A. Fragoso, *Inorg. Chim. Acta*, 468 (2017) 223-231.
35. N. Diab, D.M. Morales, C. Andronescu, M. Masoud, W. Schuhmann, *Sens. Actuators, B*, 285 (2019) 17-23.

© 2019 The Authors. Published by ESG ([www.electrochemsci.org](http://www.electrochemsci.org)). This article is an open access article distributed under the terms and conditions of the Creative Commons Attribution license (<http://creativecommons.org/licenses/by/4.0/>).